A comprehensive analysis for the shakedown of a Bree plate made of functionally graded materials

ARTICLE *in* ACTA MECHANICA · OCTOBER 2010

Impact Factor: 1.47 · DOI: 10.1007/s00707-010-0312-y

Acta Mech 214, 169–184 (2010)
DOI 10.1007/s00707-010-0312-y

X. Peng · N. Hu · H. Zheng · C. Fang

A comprehensive analysis for the shakedown of a Bree plate made of functionally graded materials

Received: 26 August 2009 / Revised: 24 November 2009 / Published online: 17 April 2010

Abstract The shakedown of a functionally graded (FG) plate subjected to coupled constant mechanical load and cyclically varying temperature is analyzed comprehensively. The material of the plate is composed of an elastoplastic matrix and elastic particles, and the particle volume fraction varies through the thickness. The distributions of the effective mechanical and thermal properties of the composites through the thickness are evaluated with mean-field approaches and described with an exponential law. The temperature dependence of the material properties is taken into account. The distribution of temperature change and the shakedown of a typical FG Bree plate are analyzed. The comparison with the results of its homogeneous counterpart and that without considering the temperature dependence of the material properties exhibits marked qualitative and quantitative difference. The effect of the temperature dependence of the elastic properties of materials is also investigated. Since FG structures are usually subject to severe coupled thermal-mechanical loadings, the approach developed and the results obtained are significant for the analysis and design of such kind of structures.

1 Introduction

Functionally graded materials (FGMs) are a class of composites characterized by the gradual variation in composition, microstructure and material properties [1]. FGMs emerged from the need to enhance material performance with the concept of taking advantages of the properties of the attendant constituents. Because of the advantages and the technical potential, FGMs have been increasingly used in many fields of the modern industries [2–4]. Motivated by increasing applications, FGMs also attracted increasing research interests in recent years, which focused mainly on the thermomechanical behavior of FGMs and the characteristics of FG structures [1,5–11]; crack and fracture [12–15]; transient thermal stress [2,16–19]; static and dynamic responses [20–27]; thermomechanical creep, instability and buckling [28–32], etc. The shakedown of an FG structure subjected to coupled varying thermal and mechanical loading was first investigated by Peng et al.

X. Peng (✉) · N. Hu · H. Zheng · C. Fang
Department of Engineering Mechanics, Chongqing University, 400044 Chongqing, China
E-mail: xhpeng@cqu.edu.cn

H. Zheng
E-mail: weiwei1001@yahoo.com.cn

C. Fang
E-mail: fcrzwj@sina.com

N. Hu
Department of Mechanical Engineering, Chiba University, 1-33 Yayoi, Inage-ku, Chiba 263-8522, Japan
E-mail: ninghu@cqu.edu.cn

[33], where, as an initial analysis and in order to avoid complexity, the temperature dependence of material properties was not taken into account. It may limit the application in the case of severe temperature change where the effect of temperature on material properties cannot be neglected. Since the shakedown is an essential problem for FG structures subjected to coupled varying thermal and mechanical loading, the corresponding approach should necessarily be developed.

The shakedown of an FG Bree plate is analyzed comprehensively in this paper. The plate is subjected to coupled constant mechanical load and cyclically varying temperature change. The material of the plate is composed of an elastoplastic matrix and elastic particles, with particle volume fraction varying through the thickness. The distributions of the effective mechanical and thermal properties of the composites are evaluated with mean-field approaches. The temperature dependence of the yield strength and the coefficient of thermal expansion (CTE) is taken into account. The boundary of elasticity and the boundaries related to incremental collapse and reversed plasticity are analyzed. The comparison with the result of the homogeneous counterparts and the result without taking into account the temperature dependence of material properties shows remarkable difference, indicating the significance of taking into account the temperature dependence of material properties in the shakedown analysis of FG structures.

2 Constitutive model and static and kinematic shakedown theorems

Assuming small deformation and for initially isotropic and plastically incompressible materials, the constitutive model adopted can be expressed as

$$\varepsilon_{ij} = \varepsilon_{ij}^{e} + e_{ij}^{p} + \varepsilon_{ij}^{\theta}, \tag{1}$$

where ε_{ij} is strain and ε_{ij}^{e}, e_{ij}^{p} and $\varepsilon_{ij}^{\theta}$are its elastic, plastic and thermal components, respectively, which are determined with

$$\varepsilon_{ij}^{e} = \frac{1}{E}\left[(1+v)\sigma_{ij} - v\sigma_{kk}\delta_{ij}\right], \quad \varepsilon_{ij}^{\theta} = \alpha(\theta-\theta_0)\delta_{ij}, \quad de_{ij}^{p} = d\lambda s_{ij}, \tag{2.1–3}$$

where E, ν and α are Young's modulus, Poisson's ratio and CTE, respectively, σ_{ij} and s_{ij} are stress and its deviatoric component, θ and θ_0 are temperature and reference temperature, respectively, δ_{ij} is the Kronecker delta, and [34]

$$d\lambda = \frac{d\zeta}{f(\lambda)s_y^0} \quad \text{with} \quad d\zeta = \sqrt{de_{ij}^{p} de_{ij}^{p}}, \tag{3}$$

s_y^0 is a material constant related to initial yield and $f(\lambda)$ is a function describing isotropic hardening. The following hardening function is adopted in the following analysis:

$$f(\lambda) = d - (d-1)\mathrm{e}^{-\beta\lambda} \quad \text{with} \quad f(0) = 1 \text{ and } d \geq 1. \tag{4}$$

Keeping in mind that λ is non-negative and non-decreasing in any plastic deformation process, it can be seen in Eqs. (3) and (4) that $f(\lambda)$ increases with the development of plastic deformation and tends to its asymptotic value d corresponding to the ultimate strength $\sigma_y = d \cdot \sigma_y^0$ as plastic deformation fully develops when $\lambda \to \infty$, indicating a saturated state of isotropic hardening. Substituting Eqs. (3) into (2.3) yields the following Mises-type yield condition:

$$s_{ij}s_{ij} = \left[f(\lambda)s_y^0\right]^2. \tag{5}$$

Introducing the loading function

$$F\left(s_{ij}, k\right) = \sqrt{s_{ij}s_{ij}} - ks_y^0, \quad \text{with} \quad 1 \leq k \leq d, \tag{6}$$

it can be seen that any state of stress should satisfy $F\left(s_{ij}, k\right) \leq 0$, and$F\left(s_{ij}, k\right) = 0$ defines a loading surface.

Given a set of actual stress and hardening states, s_{ij}, k, and a set of allowable stress and hardening states, s_{ij}^*, k^*, which satisfy

$$\begin{aligned} F\left(s_{ij}, k\right) &= 0, \quad 1 \le k \le d; \\ F\left(s_{ij}^*, k^*\right) &\le 0, \quad 1 \le k^* \le d, \end{aligned} \tag{7}$$

and making use of the following inequality

$$(s_{ij} - s_{ij}^*)de_{ij}^p \ge 0, \tag{8}$$

one can prove that [35]

$$(s_{ij}^* - s_{ij})de_{ij}^p \le s_y^0(k^* - k)d\zeta. \tag{9}$$

Static Shakedown Theorem: If there exist a time-independent residual stress field $\bar{\rho}_{ij}$ and a time-independent field k^* such that for all the load variations within a given load domain Ω, the following condition holds

$$F\left(s_{ij}^E + \bar{\rho}_{ij}, k^*\right) \le 0, \tag{10}$$

then the total energy dissipated in any allowable load path is bounded [33].

In (10) s_{ij}^E is the purely elastic solution of the deviatoric stress determined by external loads, and $1 \le k* \le d$.

Kinematic Shakedown Theorem: If there exist, over a certain time interval (t_1, t_2), a history of load resulting in a history of purely elastic stress $s_{ij}^E(\mathbf{x}, t)$, and a history of plastic strain $\bar{e}_{ij}(\mathbf{x}, t)$ resulting in a kinematically admissible increment such that

$$\Delta\bar{e}_{ij}(\mathbf{x}) = \bar{e}_{ij}(\mathbf{x}, t_2) - \bar{e}_{ij}(\mathbf{x}, t_1) = \frac{1}{2}(\Delta\bar{u}_{i,j} + \Delta\bar{u}_{j,i}), \tag{11}$$

with $\Delta\bar{u}_i = 0$ on S_u (the boundary where displacement is prescribed), and if shakedown occurs to the given structure, the condition

$$\int_{t_1}^{t_2}\int_V s_{ij}^E(\mathbf{x}, t)\dot{\bar{e}}_{ij}(\mathbf{x}, t)\mathrm{d}V\mathrm{d}t \le \int_{t_1}^{t_2}\int_V D\left(\dot{\bar{e}}_{ij}(\mathbf{x}, t)\right)\mathrm{d}V\mathrm{d}t, \tag{12}$$

should be satisfied for all kinematically admissible plastic strain cycles [33].

In (12),

$$D\left(\dot{\bar{e}}_{ij}(\mathbf{x}, t)\right) = \bar{s}_{ij}(\mathbf{x}, t)\dot{\bar{e}}_{ij}(\mathbf{x}, t) \tag{13}$$

is a dissipation function.

The following relationship was suggested for practical application by substituting Eqs. (2.3) and (3) into (12), following the definition by König [36],

$$\int_V d \cdot s_y^0\Delta\bar{\zeta}\mathrm{d}V - \sum_{k=1}^{m}\int_V \alpha_k(\mathbf{x})J_k(\mathbf{x})\mathrm{d}V \ge 0, \tag{14}$$

where

$$\Delta\bar{\zeta} = \left\|\Delta\bar{e}_{ij}\right\|, \quad J_k(\mathbf{x}) = s_{ij}^E(\mathbf{x})\Delta\bar{e}_{ij}(\mathbf{x}), \quad \alpha_k = \begin{cases} \beta_k^+ & \text{if } J_k(\mathbf{x}) > 0, \\ \beta_k^- & \text{if } J_k(\mathbf{x}) < 0, \end{cases} \tag{15}$$

and a set of inequalities $\beta_k^- \le \beta_k \le \beta_k^+ (k = 1, 2, \ldots, m)$ defines the domain Ω of loads.

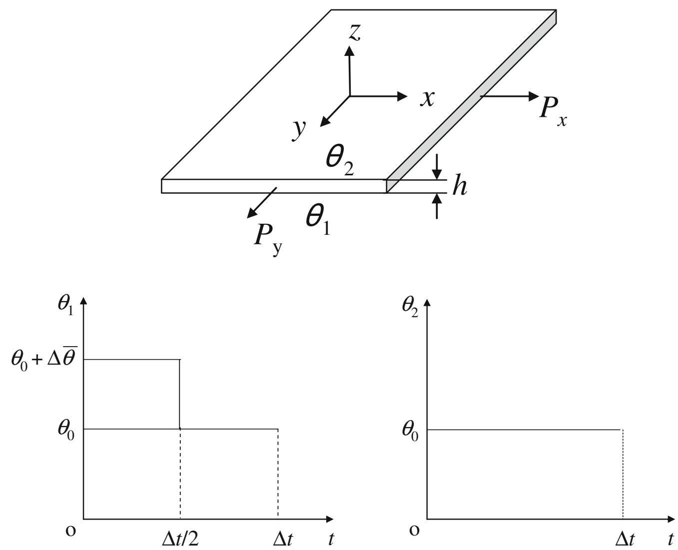

Fig. 1 The Bree plate

3 Analysis for shakedown of an FG Bree plate

A plate (Fig. 1) of thickness h is subjected to loads (P_x, P_y) per unit length in two mutually orthogonal directions. The surfaces of the plate are subjected to temperatures θ_2 and θ_1 which vary cyclically as shown in Fig. 1. The cycle time Δt is assumed large compared to the characteristic heat conduction time, and the change, between θ_0 (a reference temperature) and $\theta_0 + \Delta\bar{\theta}$, is assumed to take place sufficiently slowly for steady state conditions to prevail. The strain ε_x and ε_y are assumed to be uniform throughout the thickness of the plate. The problem is a simulation of the behavior of a thin- walled tube, in the context of a nuclear fuel can design problem by Bree [37] for homogeneous material and perfect plasticity.

3.1 Distribution and temperature dependence of material properties

In this paper, both the spatial change and the temperature-dependence of yield strength and CTE, and the special variation of thermal conductivity and Young's modulus are considered. The spatial variation and the temperature-dependence of Poisson's ratio is ignored, for its variation and effect is less significant in the interesting ranges of particle volume fraction and temperature change, but taking it into account may add much complicity to analysis. The temperature dependence of the elastic properties of the material involved is temporarily ignored in Sects. 3 and 4, because, to the authors' knowledge, no static shakedown theorem in the literature is available for materials having elastic properties varying with temperature. An exception seems to be the theorem suggested by König [38], which is, however, practically inapplicable due to its too restrictive assumption, i.e., temperature increases monotonically at every point of a structure. In the discussion in Sect. 5, the temperature dependence of the elastic properties is considered in the shakedown analyses with (1) the adopted kinematic shakedown theorem and (2) a direct extension of the adopted static shakedown theorem, and the results obtained are compared to the results without taking into account the temperature dependence of elastic property.

We assume that the material properties can be expressed as

$$C = C(z, \Delta\theta) = M(z)T(\Delta\theta), \tag{16}$$

where $M(z)$ and $T(\Delta\theta)$ describe the spatial variation and the temperature dependence of C, respectively, $\Delta\theta = \theta - \theta_0$ is temperature change, with θ and θ_0 being working temperature and reference temperature, respectively.

The spatial variation of the properties is expressed as [39]

$$M(z) = M_0 m(z), \quad m(z) = M_0^{-\left(\frac{1}{2}+\frac{z}{h}\right)} M_h^{\frac{1}{2}+\frac{z}{h}} = q^{\frac{1}{2}+\frac{z}{h}}, \quad \left(-\frac{h}{2} \le z \le \frac{h}{2}\right), \tag{17}$$

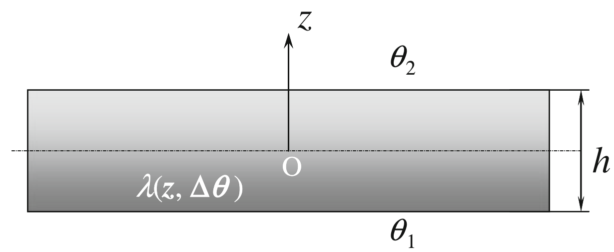

Fig. 2 Heat transfer in a Bree plate

where $M_0 = M(-h/2)$, $M_h = M(h/2)$ and $q = M_h/M_0$, respectively. Replacing M with E, α, s_y^0 and λ (thermal conductivity), replacing m with m_E, m_α, m_y and m_λ, and q with q_E, q_α, q_y and q_λ, one obtains

$$\begin{array}{llll} E(z) = E_0 m_E(z), & \alpha(z) = \alpha_0 m_\alpha(z), & s_y^0(z) = s_{y0}^0 m_s(z), & \lambda(z) = \lambda_0 m_\lambda(z) \\ m_E(z) = q_E^{\frac{1}{2}+\frac{z}{h}}, & m_\alpha(z) = q_\alpha^{\frac{1}{2}+\frac{z}{h}}, & m_y(z) = q_y^{\frac{1}{2}+\frac{z}{h}}, & m_\lambda(z) = q_\lambda^{\frac{1}{2}+\frac{z}{h}} \\ q_E = \frac{E(h/2)}{E(-h/2)}, & q_\alpha = \frac{\alpha(h/2)}{\alpha(-h/2)}, & q_y = \frac{s_y^0(h/2)}{s_y^0(-h/2)}, & q_\lambda = \frac{\lambda(h/2)}{\lambda(-h/2)}, \end{array} \quad \left(-\frac{h}{2} \le z \le \frac{h}{2}\right), \tag{18}$$

for the distributions of Young's modulus, CTE, yield strength and thermal conductivity, respectively.

The temperature dependence of yield strength and CTE takes the following linear form, assuming moderate change of temperature:

$$T_i(\Delta\theta) = a_i(\theta_0) + b_i \Delta\theta, \tag{19}$$

where a_i and b_i are material constants. The subscript i can be replaced with y and α for yield strength and CTE, respectively.

3.2 Temperature distribution

Assuming steady-state heat transfer, the distribution of the temperature can be determined with the following heat conduction equation without considering source heat:

$$\nabla \cdot \{\lambda(\mathbf{x}, \Delta\theta)\nabla\theta\} = 0. \tag{20}$$

For uniaxial heat transfer, as shown in Fig. 2, and neglecting the temperature dependence of thermal conductivity, Eq. (20) can be simplified as

$$\frac{\mathrm{d}}{\mathrm{d}z}\left\{\lambda(z)\frac{\mathrm{d}\theta}{\mathrm{d}z}\right\} = 0. \tag{21}$$

Keeping in mind Eqs. (17) and (18), and making use of the thermal boundary condition shown in Fig. 1, the distribution of temperature change can be obtained as

$$\Delta\theta(z) = \frac{(1 - q_\lambda^{\frac{1}{2}-\frac{z}{h}})}{1 - q_\lambda}\Delta\tilde{\theta}, \tag{22}$$

with

$$\Delta\tilde{\theta} = \begin{cases} 0 & (n+0.5)\Delta t \le t \le (n+1)\Delta t, \\ \Delta\bar{\theta} & n\Delta t \le t \le (n+0.5)\Delta t. \end{cases} \tag{23}$$

3.3 Purely elastic solutions of mechanical and thermal stress distributions

We will be concerned with the solution when the displacement in y-direction is fixed, i.e., $\varepsilon_y = 0$ [37]. In this case, we have

$$\sigma_x = \frac{E(z)}{1-\nu^2}\left[\varepsilon_x - \alpha(z, \Delta\theta)(1+\nu)\Delta\theta(z)\right]. \tag{24}$$

If P_x is applied individually, i.e., $\theta(z)$ is fixed at each point in the plate, the corresponding stress distribution can be obtained as

$$\sigma_P = \sigma_x|_{\Delta\tilde{\theta}=0} = \frac{E(z)}{E_0}\frac{\ln q_E}{q_E - 1}\frac{P_x}{h}, \tag{25}$$

It can be seen that the stress is no longer distributed uniformly in the cross-section because of the non-uniform distribution of the elastic property.

If $\Delta\bar{\theta}$ is applied individually, the neutral plane of the plate will not coincide with its geometrically symmetrical plane, due to the non-uniform distribution of the material properties. Assuming at the neutral plane, $z = a$, keeping in mind that $\sigma_x(a) = 0$ and $\varepsilon_x(z) = \varepsilon_x(a) = \varepsilon_0$, ε_0 can be determined with the following equation by making use of Eq. (24) and the equilibrium condition, $\int_A \sigma_x \mathrm{d}A = 0$:

$$\varepsilon_0 = \frac{(1+\nu)\int_{-h/2}^{h/2} E(z)\alpha(z, \Delta\theta)\Delta\theta(z)\mathrm{d}z}{\int_{-h/2}^{h/2} E(z)\mathrm{d}z} = \frac{\alpha_0(1+\nu)\ln q_E}{q_E - 1}\Lambda_1\left(\Delta\tilde{\theta}\right)\Delta\tilde{\theta}, \tag{26}$$

where

$$\Lambda_1\left(\Delta\bar{\theta}\right) = \frac{\Lambda_{11}\left(\Delta\tilde{\theta}\right) + \Lambda_{12}\left(\Delta\tilde{\theta}\right) + \Lambda_{13}\left(\Delta\tilde{\theta}\right) + \Lambda_{14}\left(\Delta\tilde{\theta}\right)}{(q_\lambda - 1)^3 \ln q_{\alpha E}\left(\ln q_{\alpha E} - 3\ln q_\lambda\right)\left(\ln q_{\alpha E} - 2\ln q_\lambda\right)\left(\ln q_{\alpha E} - \ln q_\lambda\right)}, \tag{27}$$

$$\begin{aligned}
\Lambda_{11}\left(\Delta\tilde{\theta}\right) &= -(q_\lambda - 1)^3\left(a_\alpha + b_\alpha\Delta\tilde{\theta}\right)(\ln q_{\alpha E})^3, \qquad q_{\alpha E} = q_\alpha q_E,\\
\Lambda_{12}\left(\Delta\tilde{\theta}\right) &= (q_\lambda - 1)^2\left[b_\alpha(4q_\lambda - 6)\Delta\tilde{\theta} + a_\alpha(5q_\lambda + q_{\alpha E} - 6)\right](\ln q_{\alpha E})^2\ln q_\lambda,\\
\Lambda_{13}\left(\Delta\tilde{\theta}\right) &= -(q_\lambda - 1)\left[a_\alpha(q_\lambda - 1)(6q_\lambda + 5q_{\alpha E} - 11) + b_\alpha\left(11 - 2q_{\alpha E} + 3(q_\lambda - 4)q_\lambda\right)\Delta\tilde{\theta}\right],\\
&\quad \ln q_{\alpha E}(\ln q_\lambda)^2,\\
\Lambda_{14}\left(\Delta\tilde{\theta}\right) &= 6(q_{\alpha E} - 1)\left[a_\alpha(1 - q_\lambda) + b_\alpha\Delta\tilde{\theta}\right](1 - q_\lambda)(\ln q_\lambda)^3.
\end{aligned} \tag{28}$$

With ε_0, a can be solved from the following equation obtained from Eq. (24)

$$\varepsilon_0 = \varepsilon_x(a, \Delta\theta(a)) = \alpha(a, \Delta\theta(a))(1+\nu)\Delta\theta(a), \tag{29}$$

and the thermal stress can be determined with

$$\sigma_\theta = \sigma_x|_{P_x=0} = \frac{E(z)}{1-\nu^2}\left[\varepsilon_0 - \alpha(z, \Delta\theta)(1+\nu)\Delta\theta(z)\right], \tag{30}$$

where $\Delta\theta(z)$ is determined with Eq. (22).

3.4 Static shakedown of the Bree plate

(1) Initial yield

No plastic deformation takes place provided

$$\begin{aligned}
&\sigma_P(z) + \sigma_\theta(z, \Delta\theta) \le \sigma_y^0(z, \Delta\theta) && \text{for} \quad a \le z \le h/2,\\
&\sigma_P(z) + \sigma_\theta(z, \Delta\theta) \ge -\sigma_y^0(z, \Delta\theta) && \text{for} \quad -h/2 \le z \le a,\\
&\text{and} \quad \sigma_P(z) \le \sigma_y^0(z, 0).
\end{aligned} \tag{31}$$

where $\sigma_y^0(z, \Delta\theta) = m_y(z)T_y(\Delta\theta)\sigma_{y0}^0$ and σ_{y0}^0 is a material constant related to the initial yield of the plate under the given loading condition. It should be noted that the boundary determined by Eq. (31) may not be linear in the $P_x - \Delta\bar{\theta}$ plane because of the non-linear nature of $\sigma_P(z)$, $\sigma_\theta(z, \Delta\theta)$ and $\sigma_y^0(z, \Delta\theta)$.

(2) Static shakedown analysis
Suppose there are a time-independent residual stress field $\bar{\rho}_x(z, \Delta\theta)$ and a time-independent field $k^*(1 \leq k^* \leq d)$ in the plate, the plate will shakedown if the following condition is satisfied:

$$\begin{array}{ll} \sigma_P(z) + \sigma_\theta(z, \Delta\theta(z)) + \bar{\rho}_x(z) \leq \sigma_y(z, \Delta\theta(z)), & a \leq z \leq h/2, \\ \sigma_P(z) + \bar{\rho}_x(z) \leq \sigma_y(z, 0), & -h/2 \leq z \leq a, \\ \sigma_P(z) + \bar{\rho}_x(z) \geq -\sigma_y(z, 0) & a \leq z \leq h/2, \\ \sigma_P(z) + \sigma_\theta(z, \Delta\theta(z)) + \bar{\rho}_x(z) \geq -\sigma_y(z, \Delta\theta(z)), & -h/2 \leq z \leq a. \end{array} \tag{32}$$

In order to derive a maximal shakedown area, $k^* = d$ is adopted in the following analysis.
The shakedown boundaries of the plate include two parts: the boundary between the area of shakedown and that of incremental collapse, and the boundary between the area of shakedown and that of reversed plasticity.

(a) Shakedown boundary corresponding to incremental collapse
Incremental collapse may take place if Eqs. (32) become

$$\begin{array}{ll} \sigma_P(z) + \sigma_\theta(z, \Delta\theta(z)) + \bar{\rho}_x(z) = \sigma_y(z, \Delta\theta(z)), & a \leq z \leq h/2, \\ \sigma_P(z) + \bar{\rho}_x(z) = \sigma_y(z, 0), & -h/2 \leq z \leq a, \\ \sigma_P(z) + \bar{\rho}_x(z) \geq -\sigma_y(z, 0) & a \leq z \leq h/2, \\ \sigma_P(z) + \sigma_\theta(z, \Delta\theta(z)) + \bar{\rho}_x(z) \geq -\sigma_y(z, \Delta\theta(z)), & -h/2 \leq z \leq a. \end{array} \tag{33}$$

Eqs. (33) indicate that, in the duration from $n\Delta t$ to $(n + 0.5)\Delta t$, at each point in the region $a \leq z \leq h/2$ of the cross section, the stress $\sigma_P(z) + \sigma_\theta(z, \Delta\theta) + \bar{\rho}_x(z)$ reaches $\sigma_y(z, \Delta\theta)$, while in the duration from $(n + 0.5)\Delta t$ to $(n + 1)\Delta t$, at each point in the region $-h/2 \leq z \leq a$ of the cross section, the stress $\sigma_P(z) + \bar{\rho}_x(z)$ reaches $\sigma_y(z, 0)$. The two parts of the cross section may flow forward alternatively.

(b) Shakedown boundary corresponding to reversed plasticity
It can be obtained from Eqs. (32) that

$$\begin{array}{ll} \sigma_\theta(z, \Delta\theta(z)) \leq \sigma_y(z, \Delta\theta(z)) + \sigma_y(z, 0) & a \leq z \leq h/2, \\ \sigma_\theta(z, \Delta\theta(z)) \geq -\sigma_y(z, \Delta\theta(z)) - \sigma_y(z, 0) & -h/2 \leq z \leq a. \end{array} \tag{34}$$

The equality of both sides of any one in Eqs. (34) at any point in the cross section implies the equality of both sides of (32.1) and (32.3), or the equality of (32.2) and (32.4), indicating that reversed plasticity occurs to this point in the cross section.

3.5 Kinematic shakedown analysis

Given a kinematically admissible strain increment $\Delta\bar{\varepsilon}$ and keeping in mind Eqs. (24) and (25), one obtains the following relationships from Eq. (15):

$$J_P = \sigma_P \Delta\bar{\varepsilon} = \frac{E(z)}{E_0} \frac{\ln q_E}{q_E - 1} \frac{P_x}{h} \Delta\bar{\varepsilon} > 0, \qquad -h/2 \leq z \leq h/2, \tag{35a}$$

$$\beta_P^- = 0, \qquad \beta_P^+ = 1, \qquad \text{so that} \qquad \alpha_P = \beta_P^+ = 1. \tag{35b}$$

Similarly, keeping in mind Eqs. (26) and (30), one obtains

$$\begin{array}{lll} J_\theta = \frac{E(z)}{1-\nu^2} \left[\varepsilon_0 - \alpha(z, \Delta\theta)\,(1+\nu)\,\Delta\theta(z)\right] \Delta\bar{\varepsilon} > 0 & \text{for } a \leq z \leq h/2, & \text{and } \alpha_\theta = \beta_\theta^+ = 1 \\ J_\theta = \frac{E(z)}{1-\nu^2} \left[\varepsilon_0 - \alpha(z, \Delta\theta)\,(1+\nu)\,\Delta\theta(z)\right] \Delta\bar{\varepsilon} < 0 & \text{for } -h/2 \leq z \leq a, & \text{and } \alpha_\theta = \beta_\theta^- = 0. \end{array} \tag{36}$$

Substituting Eqs. (35) and (36) into (14) yields the following inequality that determines the kinematic shakedown boundary:

$$d \cdot \sigma_{y0}^0 h \Lambda_2 \geq P_x + \frac{h E_0 \varepsilon_0 \Lambda_3}{1 - \nu^2} - \frac{E_0 \alpha_0 h \Delta\bar{\theta}}{1 - \nu} \sqrt{q_{\alpha E}} \frac{X_1 + X_2}{(q_\lambda - 1)^3 \ln q_{\alpha E} (\ln q_{\alpha E} - \ln q_\lambda)}, \tag{37}$$

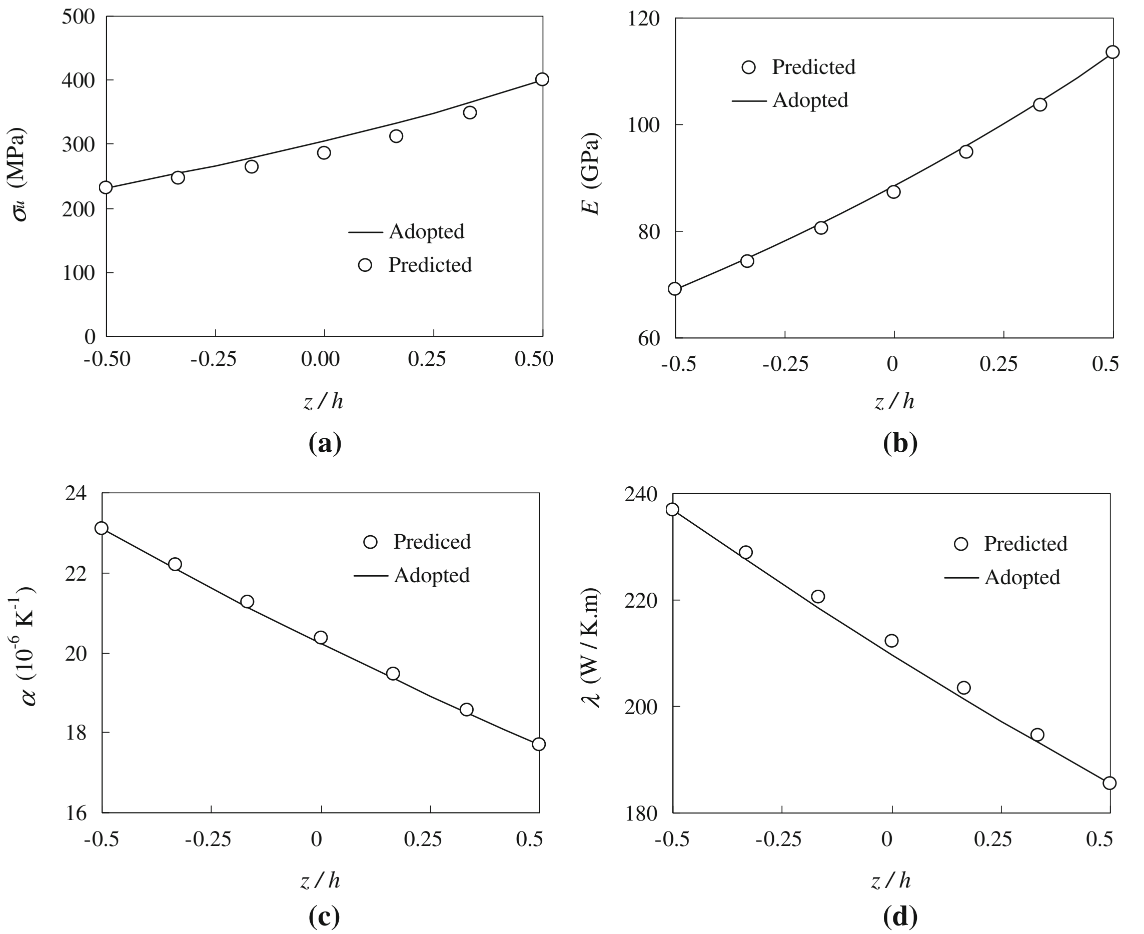

Fig. 3 Predicted and adopted mechanical properties of the Al/Al_2O_3 composite

where $\Lambda_3 = \frac{h q_E^{\frac{1}{2}}}{\ln q_E}\left(q_E^{\frac{1}{2}} - q_E^{\frac{a}{h}}\right)$,

$$\begin{aligned}
\Lambda_2 = {} & \frac{q_y^{\frac{1}{2}}}{(q_\lambda - 1)\left(\ln q_\lambda - \ln q_y\right)\ln q_y}\left\{\left[a_y\left(1 - q_\lambda\right) + b_y \Delta\bar{\theta}\right]\left(q_y^{\frac{a}{h}} - q_y^{\frac{1}{2}}\right)\ln q_\lambda\right. \\
& \left. + \left[a_y\left(q_\lambda - 1\right)\left(q_y^{\frac{a}{h}} - q_y^{\frac{1}{2}}\right) + b_y \Delta\bar{\theta}\left(q_\lambda^{\frac{1}{2}-\frac{a}{h}} - 1\right) q_y^{\frac{a}{h}}\right]\ln q_y\right\} + \frac{1}{\ln q_y}\left(q_y^{\frac{1}{2}+\frac{a}{h}} - 1\right), \qquad (38) \\
X_1 = {} & a_\alpha\left(q_\lambda - 1\right)^2 q_{\alpha E}^{\frac{a}{h}}\left[\left(1 - q_\lambda^{\frac{1}{2}-\frac{a}{h}}\right)\ln q_{\alpha E} - \left(1 - q_{\alpha E}^{\frac{1}{2}-\frac{a}{h}}\right)\ln q_\lambda\right], \\
X_2 = {} & -\frac{b_\alpha \Delta\bar{\theta}\left(q_\lambda - 1\right) q_\lambda^{-\frac{2a}{h}}}{\ln q_{\alpha E} - 2\ln q_\lambda}\left\{-2 q_{\alpha E}^{\frac{a}{h}} q_\lambda^{\frac{1}{2}+\frac{a}{h}} \ln q_{\alpha E}\left(\ln q_{\alpha E} - 2\ln q_\lambda\right)\right. \\
& \left. + q_\lambda^{\frac{2a}{h}}\left(q_{\alpha E}^{\frac{a}{h}}\left(\ln q_{\alpha E} - 2\ln q_\lambda\right)\left(\ln q_{\alpha E} - \ln q_\lambda\right) - 2\sqrt{q_{\alpha E}}\left(\ln q_\lambda\right)^2\right) + q_{\alpha E}^{\frac{a}{h}} q_\lambda \ln q_{\alpha E}\left(\ln q_{\alpha E} - \ln q_\lambda\right)\right\}.
\end{aligned}$$

Given $\Delta\bar{\theta}$, the corresponding P_x can easily be derived from Eq. (37).

Table 1 Material constants

E (GPa)		$\alpha(\times 10^{-6} K^{-1})$		σ_y^0(MPa)		λ(W/K m)		ν	d
E_0	E_h	α_0	α_h	λ_0	λ_h	σ_{y0}^0	σ_{yh}^0		
69.0	113.4	23.1	17.7	237.0	185.5	130.0	223.2	0.328	1.792

Table 2 Temperature dependence constants

α		σ_y	
a_α	b_α	a_y	b_y
1	7.091E-4	1	-1.262 E-3

4 Application to shakedown analysis of Bree plate made of Al/Al$_2$O$_3$ composite

4.1 Effective properties of the adopted material

The Bree plate is assumed to be made of functionally graded Al/Al$_2$O$_3$ composite. The thermal and mechanical properties of each constituent at 20°C and 600°C can be found in [41,42]. The effective mechanical and thermal properties of the composite are evaluated with mean field approaches.

If, in the plate, the volume fraction of particles, ξ, varies linearly from zero at the bottom surface to 30% at the top surface, the variation of σ_y and E through the thickness of the plate can be determined and shown in Figs. 3a and b, respectively, where it can be seen that the exponential rule (Eqs. (17) and (18)) can reasonably describe the distribution of σ_y and E. The average of the Poisson's ratio ν is about 0.328 and the variation and its effect is negligible. The effective CTE and thermal conductivity are evaluated respectively with [40]

$$\alpha = \alpha_m + \frac{(1/K - 1/K_m)(\alpha_c - \alpha_m)}{1/K_m - 1/K_c} \quad \text{and} \quad \lambda = \lambda_m \left[1 + \frac{\xi(\lambda_c/\lambda_m - 1)}{1 - \frac{1}{3}(1-\xi)(\lambda_c/\lambda_m - 1)} \right], \tag{39}$$

where the subscript "m" and "c" represent matrix and inclusion, respectively, K_m, K_c and K are bulk moduli of matrix, inclusion and composite, respectively. The distributions of α and λ are shown in Figs. 3c and d, respectively. The constants, which are related to Fig. 3 and used in the analysis, are listed in Table 1. With the material properties at different temperature [40,41], the temperature dependence of the CTE and the yield strength is determined and the corresponding parameters are listed in Table 2.

4.2 Determination of shakedown boundaries

Although, in principle, the lower bound of shakedown loads of a structure can be determined by simply assuming a residual stress field, in order to illustrate the importance of an appropriate shakedown analysis of FG structures, a more accurate shakedown boundary is to be achieved by taking into account in detail the effect of the non-linearity of the involved material properties and their temperature dependence on the shakedown of the FG structure.

$h = 60$ mm is used in the example. In the determination of the shakedown boundaries, the thickness of the plate is separated into 20 segments with identical increment, containing 21 points with coordinates $-h/2, \ldots, -h/2 + (k-1)h/20, \ldots, h/2, k = 1, 2, \ldots, 21$. The conditions, which should be satisfied over the thickness, are reduced to be satisfied at each point.

The boundary of pure elasticity can be determined with Eqs. (25), (30) and (31) and shown with the lines marked with (E-S) in Fig. 4. The boundary consists of three segments, determined by the three inequalities in Eq. (31), respectively. The distributions of $\sigma_P, \sigma_\theta, \sigma = \sigma_P + \sigma_\theta$, and σ_y^0 at Points A, B, C, and D in Fig. 4 are shown in Figs. 5a, b, c and d, respectively. In Fig. 5 and in the following, the zone bounded by "*" denotes the elastic zone as $\Delta\bar{\theta}$ is applied, and the zone bounded by "$\times$" denotes the elastic zone as $\Delta\bar{\theta}$ is removed, and $a' = a/h$. At point A (Fig. 4), $P_x = 0$ (or $\sigma_P = 0$), $\sigma = \sigma_\theta$ reaches $-\sigma_y^0$ at the bottom surface. At point B (Fig. 4), $\sigma = \sigma_P + \sigma_\theta$ reaches σ_y^0 at the upper surface while $\sigma = \sigma_P + \sigma_\theta$ reaches -σ_y^0 at the bottom surface. At point C (Fig. 4), $\sigma = \sigma_P + \sigma_\theta$ reaches σ_y^0 at the upper surface as $\Delta\bar{\theta}$ is applied, while $\sigma = \sigma_P + \sigma_\theta$ reaches σ_y^0 the lower surface as $\Delta\bar{\theta}$ is removed. At point D, $\Delta\bar{\theta} = 0$, $\sigma = \sigma_P$ equals σ_y^0 at the lower surface.

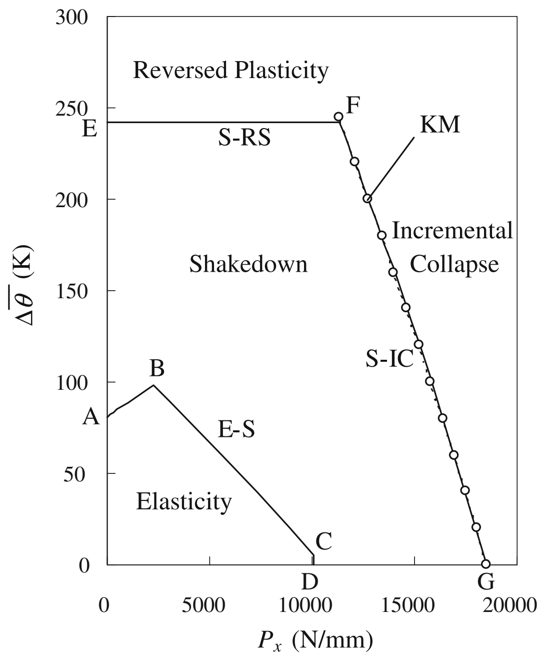

Fig. 4 Shakedown area of the Bree plate made of Al/Al_2O_3

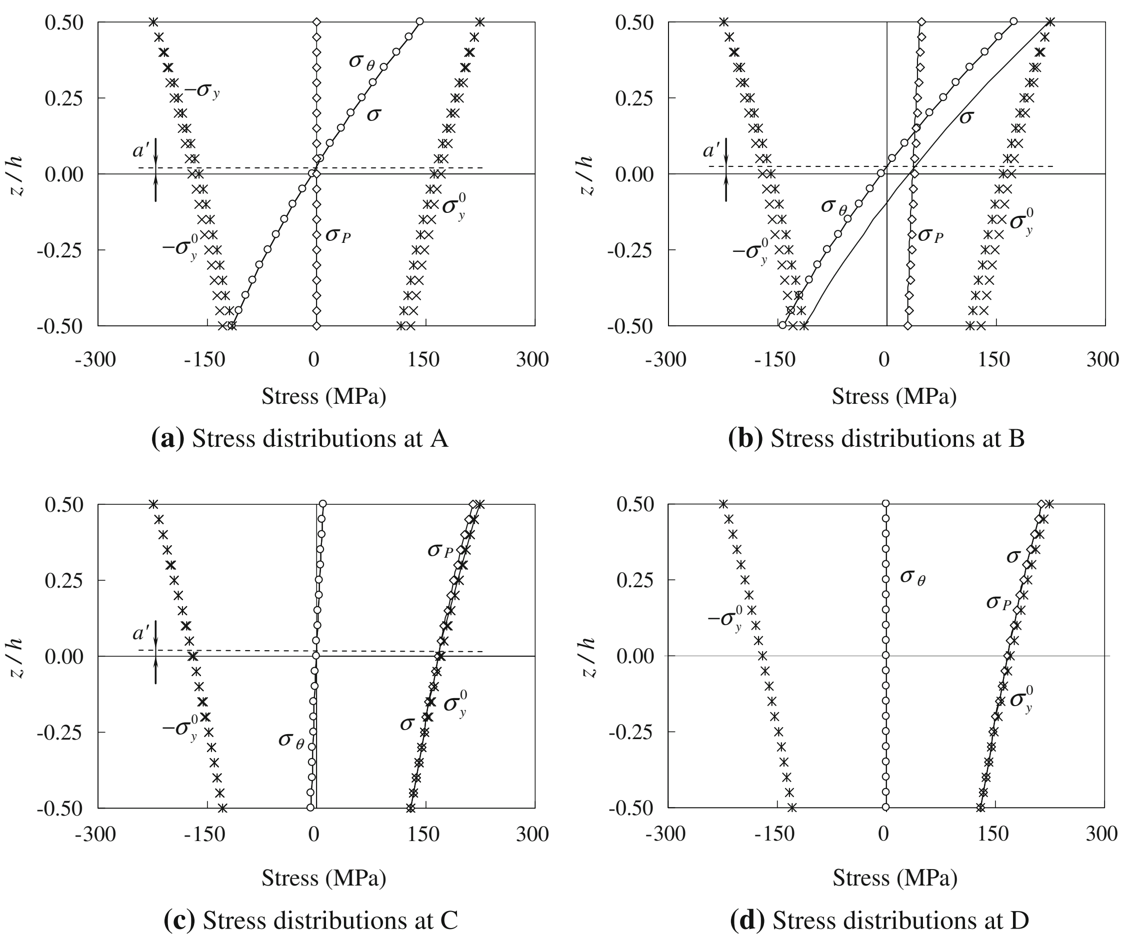

Fig. 5 Stress distributions at points A, B, C, and D in Fig. 4

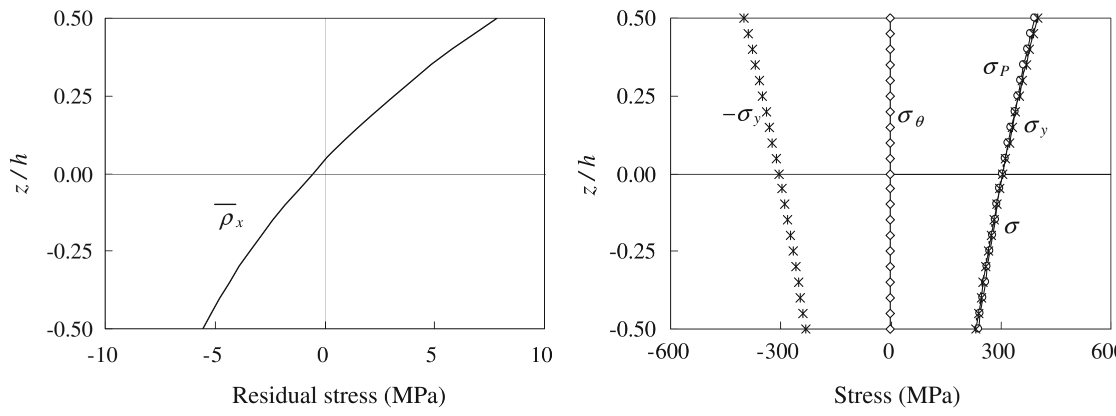

(a) Residual stress filed **(b)** Stress distributions

Fig. 6 Stress distributions at point G (Fig. 4)

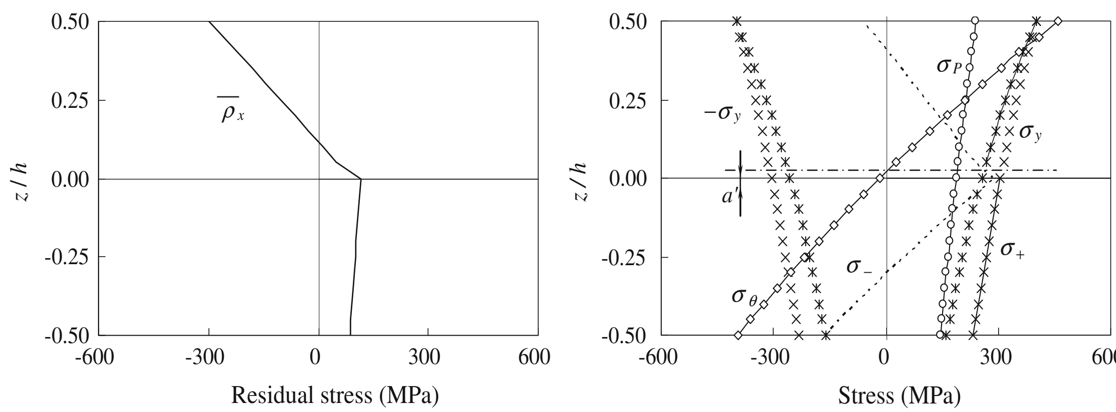

(a) Residual stress filed **(b)** Stress distributions

Fig. 7 Stress distributions at point F (Fig. 4)

The boundary between shakedown and incremental collapse areas can be determined with Eqs. (33) by the following steps: (a) Given a set of $\Delta\bar{\theta}$and P_x, the residual stress $\bar{\rho}_x$ can be estimated with the first two equations in (33); (b) Check if the obtained residual stress field $\bar{\rho}_x$ satisfies the last two inequalities in (33); (c) Check if the residual stress field $\bar{\rho}_x$ satisfies the self-equilibrium condition; and (d) if (b) or (c) is not satisfied, adjust P_x and then return to step (a). The determined boundary between shakedown and incremental collapse areas is given in Fig. 4 with the line marked with (S-IC). The distributions of the residual stress $\bar{\rho}_x$, the stress σ_P, σ_θ, and σ_+ determined by the LHS of Eqs. (33.1) and (33.2), and σ_- determined with (33.3) and (33.4), at point G (Fig. 4) are shown in Fig. 6, where plastic deformation may take place if either σ_+ or σ_- reaches the boundary. It can be seen that making use of the residual stress $\bar{\rho}_x$ shown in Fig. 6a, the obtained σ_+ throughout the thickness of the plate reaches the yield stress σ_y, indicating plastic flow takes place in the direction of σ_+. In the opposite direction, σ_- is far from $-\sigma_y$ throughout the thickness, indicating no plastic flow will occur in the direction.

Different from the results shown in Fig. 6, corresponding to $\Delta\bar{\theta} = 0$, the results corresponding to point F (Fig. 4) are given in Fig. 7. Making use of the time-independent residual stress field shown in Fig. 7a, incremental plastic deformation in the direction of P_x can be obtained in each cycle of $\Delta\bar{\theta}$. It can be seen that the stress σ_+ determined by the LHS of Eq. (33.1) reaches σ_y (the zone bounded by "*") in the region $a \leq z \leq h/2$ as $\Delta\bar{\theta}$ is applied, and the stress determined by the LHS of Eq. (33.2) reaches σ_y (the boundary bounded by "×") in the region $-h/2 \leq z \leq a$ as $\Delta\bar{\theta}$ is removed, alternatively. It implies that plastic flow takes place in the direction of P_x in the region $a \leq z \leq h/2$ during $n\Delta t$ and $(n + 0.5)\Delta t$; and in the region $-h/2 \leq z \leq a$ during $(n + 0.5)\Delta t$ and $(n + 1)\Delta t$). In the opposite direction, σ_- reaches $-\sigma_y$ at $z = -h/2$, indicating plastic

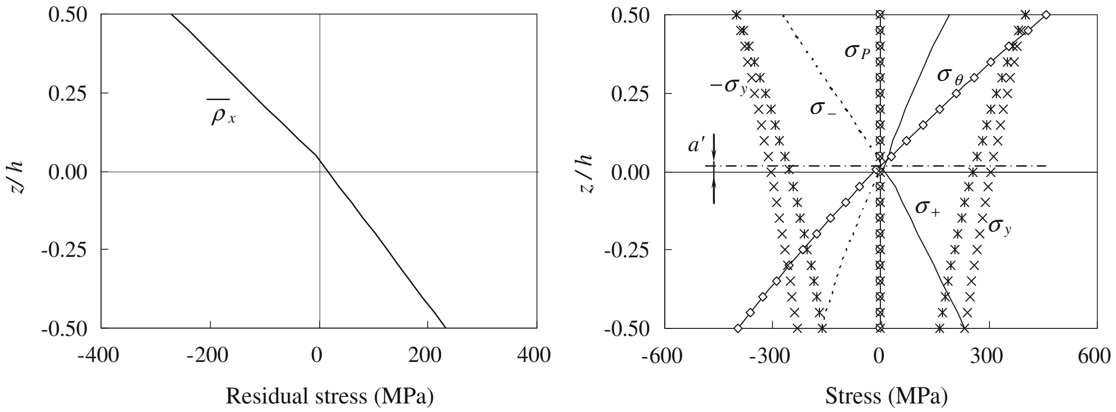

(a) Residual stress filed **(b)** Stress distributions

Fig. 8 Stress distributions at point E in Fig. 4

deformation may occur at the lower surface, but in the other part of the section, the deformation in the direction of σ_- keeps purely elastic, implying that no overall plastic deformation takes place in the direction of σ_-. Plastic deformation develops in each cycle of $\Delta\bar{\theta}$ and increases monotonically with the increase of n.

The distributions of the residual stress $\bar{\rho}_x$, the stress σ_P, σ_θ, and σ_+ determined by the LHS of Eqs. (32.1) and (32.2) and σ_- determined by the LHS of Ines. (32.3) and (32.4) under the condition of Ine. (34) are shown in Fig. 8, respectively, corresponding to point E on the line marked with S-RP (the boundary between the area of shakedown and that of reversed plasticity) in Fig. 4. In the duration when $\Delta\bar{\theta}$ is applied, the obtained σ_- reaches $-\sigma_y$ at the lower surface, indicating that reversed plastic deformation may take place at this location. It should be noted that, similar situation also occurs at point F in Fig. 4, the intersection of line S-IC and line S-RP, corresponds to the thermal-mechanical loads resulting in overall incremental collapse and local reversed plasticity.

The kinematic shakedown boundary determined with Ine. (37) is also given in Fig. 4 with dashed-circle line marked with KM. It well coincides with the boundary marked with S-IC determined by static shakedown analysis, indicating that S-IC should be a sufficiently exact shakedown boundary of this plate.

4.3 Comparison with the result of its homogeneous counterpart

In order to illustrate the difference between the result of the FG Bree plate and that of its counterpart made of homogeneous materials, the shakedown boundaries of the Bree plate made of a homogeneous material is also investigated, with the same material model, but the averaging material properties defined as

$$\begin{aligned}
\bar{E} &= \tfrac{1}{h}\int_{-h/2}^{h/2} E(z)\mathrm{d}z = \tfrac{q_\mu-1}{\ln(q_\mu)}E_0, \quad \bar{\alpha} = \tfrac{1}{h}\int_{-h/2}^{h/2} \alpha(z)\mathrm{d}z = \tfrac{q_\alpha-1}{\ln(q_\alpha)}\alpha_0,\\
\bar{\sigma}_y^0 &= \tfrac{1}{h}\int_{-h/2}^{h/2} \sigma_y^0(z)\mathrm{d}z = \tfrac{q_s-1}{\ln(q_s)}\sigma_{y0}^0, \quad \bar{\lambda} = \tfrac{1}{h}\int_{-h/2}^{h/2} \lambda(z)\mathrm{d}z = \tfrac{q_\lambda-1}{\ln(q_\lambda)}\lambda_0,
\end{aligned} \tag{40}$$

With the material constants given in Table 1 and Eq. (40), these averaging properties can be determined as

$$\bar{E} = 89.377\text{GPa}, \quad \bar{\alpha} = 2.03\times10^{-5}\text{K}^{-1}, \quad \bar{\sigma}_y^o = 309.02\text{MPa}, \quad \bar{\lambda} = 209.93\text{W/K}\cdot\text{m}.$$

The purely elastic solution of the mechanical and thermal stress is obtained as

$$\sigma_P = \frac{P_x}{h}, \qquad \sigma_\theta = \frac{2z}{h}\tilde{\sigma}_\theta, \qquad \text{with} \quad \tilde{\sigma}_\theta = \frac{\bar{\alpha}\bar{E}}{2(1-\nu)}\Delta\bar{\theta}. \tag{41}$$

Given simple residual stress fields (Fig. 9), corresponding respectively to incremental collapse and reversed plasticity, the shakedown boundaries can be determined and shown with solid lines in Fig. 10. In Fig. 9b,

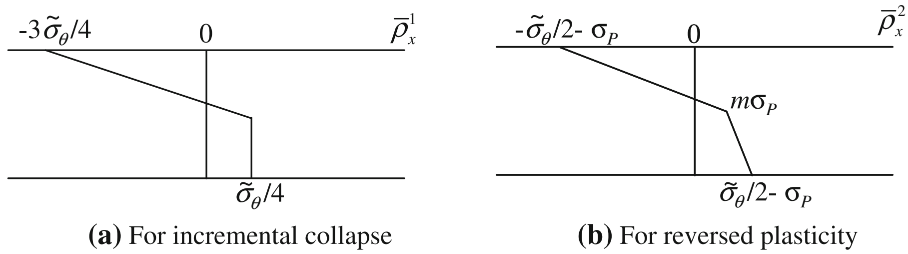

Fig. 9 Residual stress fields

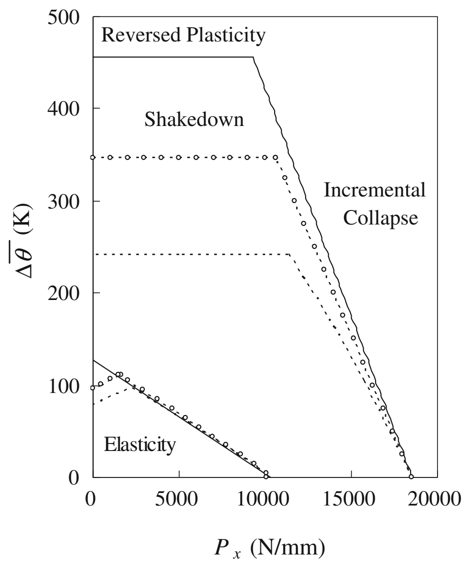

Fig. 10 Shakedown areas of the Bree plate made of equivalent homogeneous material

the parameter m can be determined by the self-equilibrium condition. Comparing the shakedown boundaries shown in Fig. 10 with that given in Fig. 4 (also exhibited in Fig. 10 with dashed lines), a remarkable difference can be observed.

4.4 Comparison with the result without considering the temperature dependence of material properties

In order to assess the effect of temperature dependence of material properties on the shakedown boundary, the shakedown boundaries of the FG Bree plate are also analyzed with the material constants in Table 1 but without taking into account the temperature dependence of material properties. The result is also shown in Fig. 10 with dashed-circle lines. It can be seen that, the boundary between the area of shakedown and that of reversed plasticity hoists markedly. The boundary of elasticity also changes distinctly. These differences indicate the significance of taking into account the temperature dependence of material properties in the shakedown analysis of FG structures.

5 Conclusions and discussion

The shakedown of a Bree plate is comprehensively analyzed. The effective thermal and mechanical properties of the composite are obtained with mean-field approaches. The material properties distribute approximately exponentially over the thickness. The effect of temperature on yield strength and CTE is considered. The temperature distribution is obtained with heat conduction equation. As an example, the shakedown of an Al/Al_2O_3 FG Bree plate is analyzed.

The shakedown boundary of the FG Bree plate exhibits distinct difference from that of its homogeneous counterpart and that without taking into account the effect of temperature on the yield strength and CTE in the

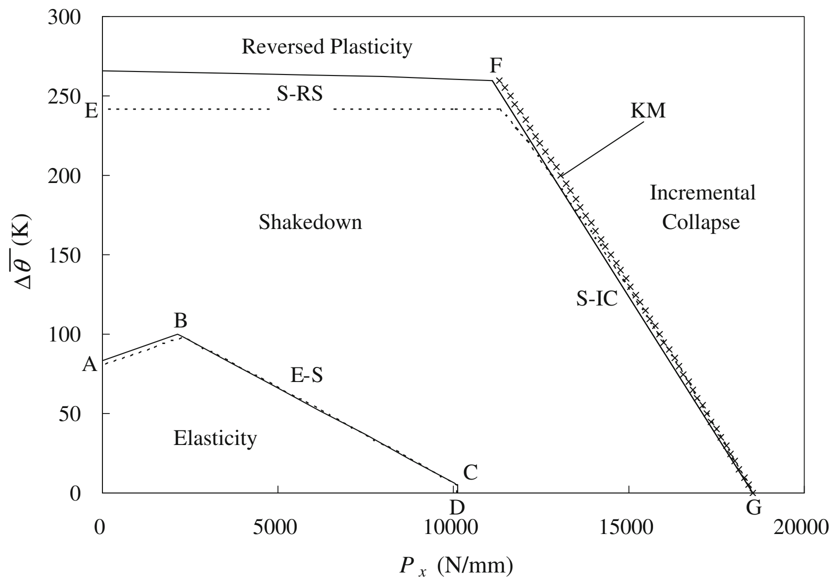

Fig. 11 Comparison between the shakedown boundaries of the Bree plate obtained with different approaches

following main aspects: (1) For the FG Bree plate, the pure elasticity boundary is no longer a straight line, but consists of several segments, corresponding to different yield criteria; (2) the homogeneous counterpart may markedly overestimates the shakedown boundary, which may result in a improper failure of the structure; and (3) the temperature dependence of the material properties plays an important role in the shakedown analysis of the FG Bree plate and should be included in the shakedown analysis.

The shakedown capability of an FG structure is determined by both the structure geometry and the distribution of material properties, which implies the possibility to enhance the shakedown capability of a structure by optimizing the properties of the attendant constituents as well as the distribution of overall material properties. It should also be noted that FG structures are usually subjected to coupled severe mechanical and thermal loads, and shakedown is an essential problem of such kind of structures, the approach developed and the results obtained are, therefore, significant for the analysis and design of FG structures.

In the above analysis, the temperature dependence of Young's modulus E was ignored. However, in the case where temperature changes in a wide range, such effects might be rather remarkable. In order to estimate the effect in the shakedown analysis, two additional approaches are adopted: (1) the kinematic shakedown theorem taking into account the temperature dependence of E, and (2) a direct extension of the static shakedown theorem to the case involving the temperature dependence of E. The results obtained are compared with that in Sect. 4.

The temperature dependence of E is also described with Eqs. (16) and (19), with $a_E = 1$ and $b_E = -5.32\text{E} - 4$, identified with the experimental data [40,41]. The shakedown boundaries of the Bree plate under the conditions identical with that in Sect. 4 are determined and shown in Fig. 11 (with solid line for the result by approach (2) and "$\times$" by for that by approach (1)). The results obtained in Sect. 4 are also shown in Fig. 11 with dashed lines for comparison.

For the boundaries related to incremental collapse, it can be seen that taking into account the temperature dependence of E may slightly decrease the shakedown area at moderate temperature, but slightly increase the shakedown area if the temperature approaches that when reversed plasticity occurs. Compared with the boundary determined by the kinematic shakedown theorem taking into account the temperature dependence of E, it can be seen that both the static shakedown theorem and its extension can provide reasonable approximations.

For the boundary related to reversed plasticity, there is a distinct difference between the boundaries with and without considering the temperature dependence of E. However, the approach without taking into account the temperature dependence of E seems to give more conservative boundary than its extension.

The distributions of ρ_x, σ_θ, σ_P, σ_+, σ_-, and σ_y at point F (Fig. 11) determined by the extension of the static shakedown theorem are shown in Fig. 12, where the reduction of E at the lower surface is about 13%. Compared with the results shown in Fig. 7, it can be seen that σ_θ and σ_P change from 483 and 252 MPa to 459 and 241 MPa, respectively at the upper surface, and change from -378 and 143 MPa to -395 and 147 MPa,

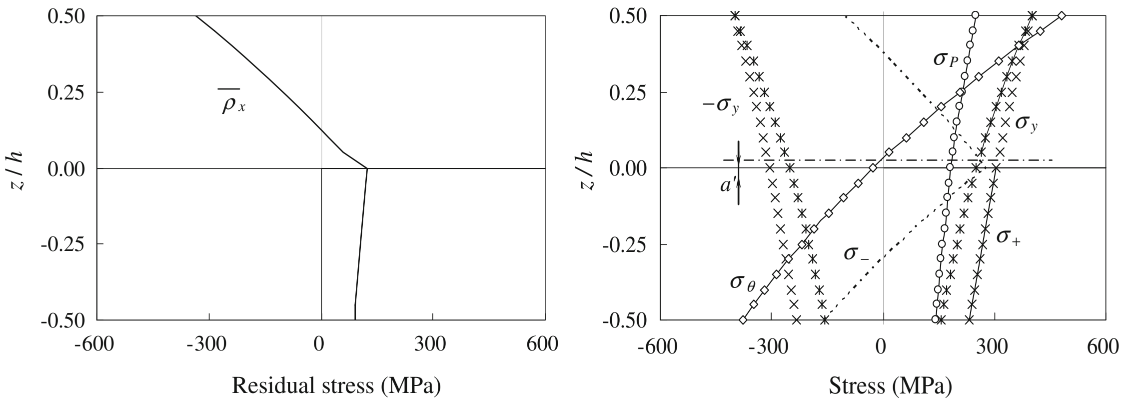

Fig. 12 Stress distributions at point F (Fig. 11)

respectively, at the lower surface, correspondingly the residual stress ρ_x changes from -334 to -300 MPa at the upper surface, and from 90 to 86.2 MPa at the lower surface. The temperature dependence of E may induce additional change in thermal-mechanical stresses due to the additional change of material properties and redistribution of stress. For instance, it may markedly reduce the thermal stress at elevated temperature, accounting for the higher boundary of reversed plasticity, as shown in Fig. 11.

Acknowledgments The authors gratefully acknowledge the financial support to this work from NSFC under Grant Number 10976032 and JSPS under Grant Number L08538.

References

1. Ilschner, B.: Processing-microstructure-property relationships in graded materials. J. Mech. Phys. Solids **44**(5), 647–656 (1996)
2. Praveen, G.N., Chin, C.D., Reddy, J.N.: Thermoelastic analysis of functionally graded ceramic-metal cylinder. J. Eng. Mech. **125**, 1259–1267 (1999)
3. Fujihara, K., Teo, K., Gopal, R., Loh, P.L., Ganesh, V.K., Ramakrishna, S., Foong, K.W.C., Chew, C.L.: Fibrous composite materials in dentistry and orthopaedics: review and applications. Compos. Sci. Technol. **64**, 775–788 (2004)
4. Wataria, F., Yokoyama, A., Omori, M., Hirai, T., Kondo, H., Uo, M., Kawasaki, T.: Biocompatibility of materials and development to functionally graded implant for bio-medical application. Compos. Sci. Technol. **64**, 893–908 (2004)
5. Shabana, Y.M., Noda, N.: Numerical evaluation of the thermomechanical effective properties of a functionally graded material using the homogenization method. Int. J. Solids Struct. **45**, 3494–3506 (2008)
6. Tanigawa, Y.: Some basic thermoelastic problems for nonhomogeneous structural materials. Appl. Mecha. Rev. **48**(6), 287–300 (1995)
7. Kim, K.S., Noda, N.: Green's function approach to solution of transient temperature for thermal stresses of functionally graded material. Int. J. Ser. A Solids Mech. Mater. Eng. **44**(1), 31–36 (2001)
8. Loy, C.T., Lam, K.Y., Reddy, J.N.: Vibration of functionally graded cylindrical shells. Int. J. Mech. Sci. **41**(3), 309–324 (1999)
9. Yang, J., Shen, H.S.: Dynamic response of initially stressed functionally graded rectangular thin plates. Compos. Struct. **54**(4), 497–508 (2001)
10. Weng, G.J.: Effective bulk moduli of two functionally graded composites. Acta Mech. **166**, 57–67 (2003)
11. Ghosh, M.K., Kanoria, M.: Analysis of thermoelastic response in a functionally graded spherically isotropic hollow sphere based on Green—Lindsay theory. Acta Mech. **207**, 51–67 (2009)
12. Wang, B., Han, J., Du, S.Y.: Crack problems for functionally graded materials under transient thermal loading. J. Therm. Stress. **23**(2), 143–168 (2000)
13. Li, C., Weng, G.J., Duan, Z., Zou, Z.: Dynamic stress intensity factor of a functionally graded material under antiplane shear loading. Acta Mech. **149**, 1–10 (2001)
14. Ueda, S.: A cracked functionally graded piezoelectric material strip under transient thermal loading. Acta Mech. **199**, 53–70 (2008)
15. Amit, K.C., Kim, J.H.: Interaction integrals for thermal fracture of functionally graded materials. Eng. Fract. Mech. **75**, 2542–2565 (2008)
16. Noda, N.: Thermal stresses in functionally graded materials. J. Therm. Stress. **22**, 477–512 (1999)
17. Ootao, Y., Tanigawa, Y.: Three-dimensional solution for transient thermal stresses of an orthotropic functionally graded rectangular plate. Compos. Struct. **80**(1), 10–20 (2007)
18. Marin, L., Lesnic, D.: The method of fundamental solutions for nonlinear functionally graded materials. Int. J. Solids Struct. **44**, 6878–6890 (2007)
19. Noda, N., Guo, L.-C.: Thermal shock analysis for a functionally graded plate with a surface crack. Acta Mech. **195**, 157–166 (2008)

20. Elishakoff, I., Gentilini, C.: Three-dimensional flexure of rectangular plates made of functionally graded materials. J. Appl. Mech. **72**(5), 788–791 (2005)
21. Zhong, Z., Shang, E.T.: Three-dimensional exact analysis of simply supported functionally gradient piezoelectric plates. Int. J. Solids Struct. **40**(20), 5335–5352 (2003)
22. Zhang, Z.J., Paulino, G.H.: Cohesive zone modelling of dynamic failure in homogeneous and functionally graded materials. Int. J. Plast. **21**(6), 1195–1254 (2005)
23. Ying, J., Lu, C.F., Chen, W.Q.: Two-dimensional elasticity solutions for functionally graded beams resting on elastic foundations. Compos. Struct. **84**, 209–219 (2008)
24. Liew, K.M., Kitipornchai, S.: Analysis of thermal stress behavior of functionally graded hollow circular cylinders. Int. J. Solids Struct. **40**, 2355–2380 (2003)
25. Eslami, M.R., Babaei, M.H., Poultangari, R.: Thermal and mechanical stresses in a functionally graded thick sphere. Int. J. Press. Vessels Pip. **82**, 522–527 (2005)
26. Li, X.Y., Ding, H.J., Chen, W.Q.: Axisymmetric elasticity solutions for a uniformly loaded annular plate of transversely isotropic functionally graded materials. Acta Mech. **196**, 139–159 (2008)
27. Pao, Y.-H., Chen, W.-Q.: Elastodynamic theory of framed structures and reverberation-ray matrix analysis. Acta Mech. **204**, 61–79 (2009)
28. Yang, J., Liew, K.M., Wu, Y.F., Kitipomchai, S.: Thermo-mechanical post-buckling of FGM cylindrical panels with temperature dependent properties. Int. J. Solids Struct. **43**(2), 307–324 (2006)
29. Na, K.S., Kim, J.H.: Three-dimensional thermomechanical buckling analysis for functionally graded composite plates. Compos. Struct. **73**(4), 413–422 (2006)
30. Feldoman, E., Aboudi, J.: Buckling analysis of functionally graded plates subjected to uniaxial loading. Compos. Struct. **38**, 29–36 (1997)
31. You, L.H., Ou, H., Zheng, Z.Y.: Creep deformations and stresses in thick-walled cylindrical vessels of functionally graded materials subjected to internal pressure. Compos. Struct. **78**, 285–291 (2007)
32. Sofiyev, A.H.: Dynamic buckling of functionally graded cylindrical thin shells under non-periodic impulsive loading. Acta Mech. **165**, 151–163 (2003)
33. Peng, X., Zheng, H., Hu, N., Fang, C.: Static and kinematic shakedown analysis of FG plate subjected to constant mechanical load and cyclically varying temperature change. Compos. Struct. **91**(2), 212–221 (2009)
34. Peng, X., Fan, J., Zeng, X.: Analysis for Plastic buckling of thin-walled cylinders via non-classical constitutive theory of plasticity. Int. J. Solids Struct. **33**(30), 4495–4509 (1996)
35. Peng, X., Ponter, A.R.S.: Extremal properties of endochronic plasticity, part II: extremal path of the endochronic constitutive equation with a yield surface and application. Int. J. Plast. **9**, 567–581 (1993)
36. König, J.A.: Shakedown of Elastic-Plastic Structures. PWN-Polish Scientific Publishers, Warsaw (1987)
37. Bree, J.: Elastic plastic behavior of thin tubes subjected to internal pressure and intermittent high heat fluxes with application to fast nuclear reactor fuel elements. J. Strain Anal. **2**, 226–238 (1967)
38. König, J.A.: A shakedown theorem for temperature dependent elastic moduli. Bull. Ac. Pol. Sci. Ser. Sci. Technol. **17**, 161 (1968)
39. Sankar, B.V.: An elasticity solution for functionally graded beams. Compos. Sci. Technol. **61**(5), 689–696 (2001)
40. Cho, J.R., Oden, J.T.: Functionally graded material: a parametric study on thermal-stress characteristics using the Crank-Nicolson-Galerkin scheme. Comput. Methods Appl. Mech. Eng. **188**, 17–38 (2000)
41. Shen, Y.L.: Thermal expansion of metal—ceramic composites: a three-dimensional analysis. Mater. Sci. Eng. A **252**, 269–275 (1998)
42. Kuromitsu, T., Yoshida, H., Takebe, H., Morinaga, K.: Interaction between alumina and binary glasses. J. Am. Ceram. Soc. **80**(6), 1583–1587 (1997)